

Electronic Supplementary Information (ESI)

***In-situ* integration of graphene foam-titanium nitride based bio-scaffolds and microfluidic structures for soil nutrient sensors**

Md. Azahar Ali,¹ Kunal Mondal,² Yifei Wang,¹ Huawei Jiang,¹ Navreet K. Mahal,³
Michael J. Castellano,³ Ashutosh Sharma,⁴ and Liang Dong^{1,*}

¹Department of Electrical and Computer Engineering, Iowa State University, Ames, Iowa 50011, USA

²Department of Chemical and Biomolecular Engineering, North Carolina State University, Raleigh, North Carolina 27695, USA

³Department of Agronomy, Iowa State University, Ames, Iowa 50011, USA

⁴Department of Chemical Engineering, Indian Institute of Technology Kanpur, Kanpur 208016, India

*Corresponding author (L.D.): E-mail: ldong@iastate.edu; Tel: +1-515-294-0388

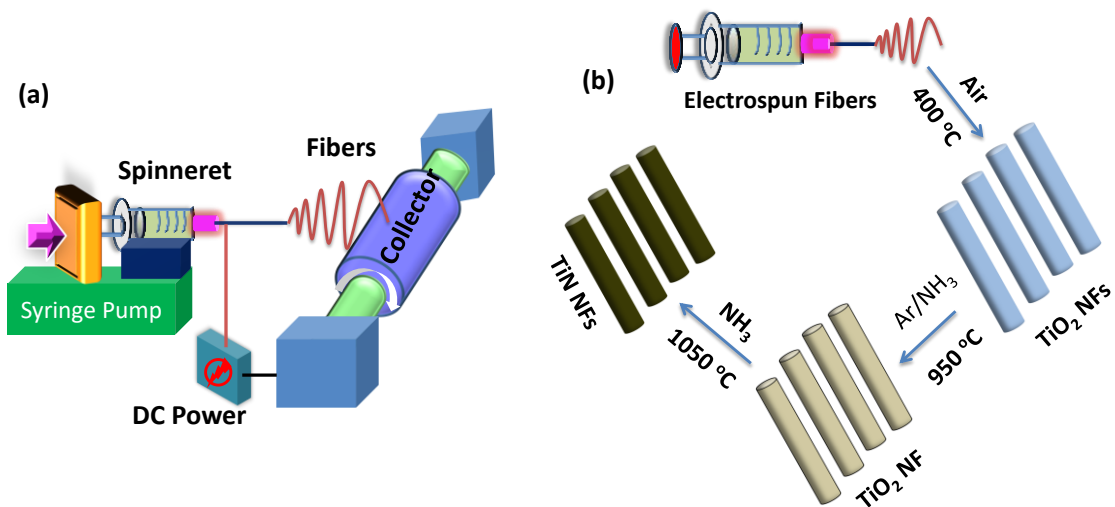


Figure S1. (a) Schematic representation of electrospinning setup. (b) Schematic representation of synthesizing TiN NFs.

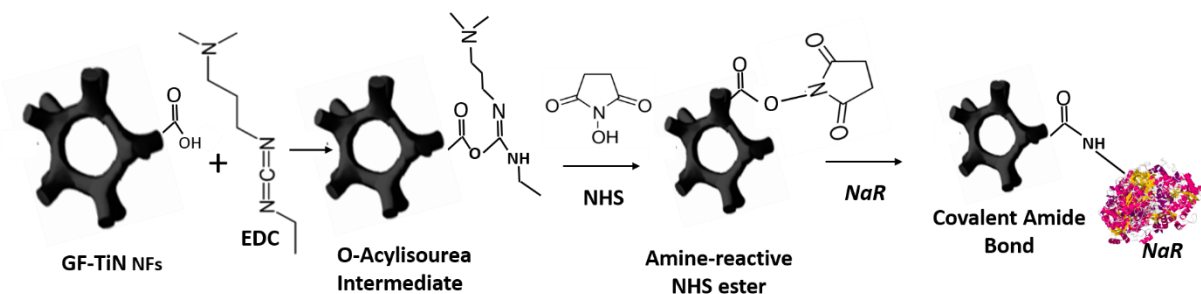


Figure S2. Pictorial representation for functionalization of carboxylated GF-TiN NFs with NaR enzyme molecules by EDC-NHS coupling method.

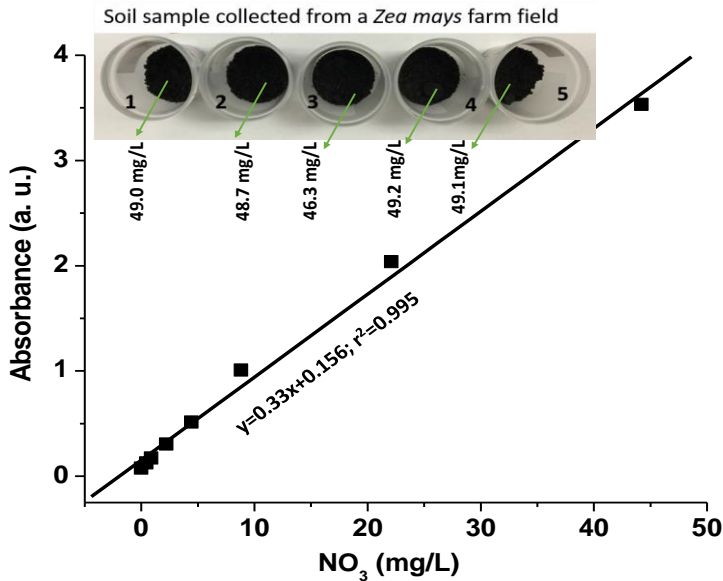


Figure S3. Photometric response for the detection of nitrate ions (0-44.2 mg/L or ppm). The inset shows the nitrate concentrations of the extracted samples from soils, as well as the soils in specimen cups.

Extraction of nitrate ions from soil samples followed our previous method.^{S5,S6} Briefly, soil samples were obtained from a *Zea mays* farm field with different intensities of artificial drainage. By weighing 10 g of field moist soil, the soil moisture content of each sample was evaluated in an aluminum boat. At 105 °C, the collected samples were dried until constant mass, and the gravimetric moisture content was estimated by mass of water per unit mass of dry soil (g/g). Subsequently, 10-15 g of field moist soil was balanced in five specimen different cups. 2.0 M potassium chloride (KCl) solution (50 mL) was mixed to all five soil samples and shaken for 1 hr. The high concentration of KCl was used due to complete extraction of nitrate ions from the soil samples. Finally, all five solutions were filtered using Whatman #1 paper and kept frozen before being used in electrochemical sensing.

To evaluate the concentration of nitrate ions that extracted from soils, a standard stock solution (1000 mg/L) of KNO₃ was prepared and diluted into several concentrations ranging from 0 to 44.2 mg/L of NO₃⁻. Separately, 50 µL of each standard stock solution and soil extracts were pipetted into a 96-well microplate using an electronic pipette. Then, 250 µL of VCl₃/Griess-Ilosvay reagent was added into each microplate well and kept at dark condition for 24 hrs in order to complete reaction. The absorbance signals recorded of this prepared 96-well microplate at a fixed wavelength of 540 nm of monochromatic light using a PowerWaveX Select Scanning Microplate Spectrophotometer. The absorbance signal is found to

increase with the increasing the concentration of nitrate ions (Fig. S3). According to obtained linear relation of absorbance-concentration plot for known standards, the concentrations for unknown soil nitrate ions were estimated. The inset of Fig. S3 shows the concentrations of NO_3^- obtained from the extracted soil samples. One of these was used by diluting into different concentrations from 0.044 to 44.2 mg/L to characterizing the sensor performances.

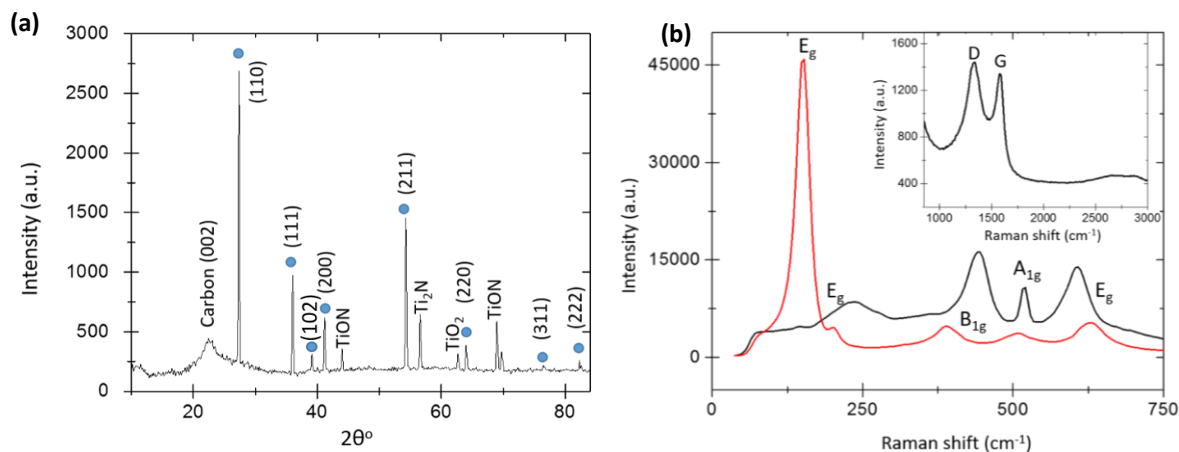


Figure S4: (a) X-ray diffraction spectrum of TiN NFs. (b) Raman spectra for pure synthesized TiO_2 NFs and TiN NFs. Inset shows the spectra from 100 cm^{-1} to 3700 cm^{-1} .

To investigate the nanocrystallinity of synthesized TiN NFs produced from electrospun TiO_2 NFs, the XRD studies were undertaken. In Fig. S4a, the observed peaks are indexed to be face-centered cubic and the 2θ angles are well accorded with the JCPDS #38-1420 data and the other literature.^{51,52} Several crystallographic planes (110, 111, 200, 211, etc.) due to the formation of cubic TiN with a lattice parameter of 4.234 \AA , and other planes due to existence of small fraction of Ti_2N , TiON, and rutile TiO_2 phase, were observed.⁵¹⁻⁵² Since we utilized heat treatment at ambient pressure, Ti_2N was formed and also the conversion of TiO_2 to TiN during heating at ammonia atmosphere perhaps incorporated a trace amount of oxygen into TiN leading to the formation of small fraction of TiON or even TiO_2 . At a higher pressure, an amount of oxygen from background gas may lead to the formation of oxides and oxynitrides, hence we avoided high pressure or low pressure furnace for heat treatment.

In Raman spectrum of TiN NFs (Fig. S4b), the scattering (acoustic range) is mostly governed by the vibrations of the Ti ions (usually $140\text{-}360 \text{ cm}^{-1}$) and in the optical phonon range by the vibrations of the N

ions ($560\text{--}670\text{ cm}^{-1}$).^{S3,S4} The peaks at 236 and 619 cm^{-1} arise due to first order transverse acoustic and transverse optical longitudinal modes of TiN NFs, respectively. Due to the presence of trace amount of oxide layer formation on the surface of TiN, two additional peaks were observed such as at 442 cm^{-1} is a signature of TiON and at 522 cm^{-1} is a typical characteristics of rutile TiO₂ NFs.^{S3,S4} Features at 150 , 207 , 390 , 512 and 632 cm^{-1} indicate the of anatase phase of TiO₂ NFs. Two peaks at 1335 and 1578 cm^{-1} conforming to the D and G bands for carbon, respectively, which reveals the presence of amorphous carbon at TiN NFs.

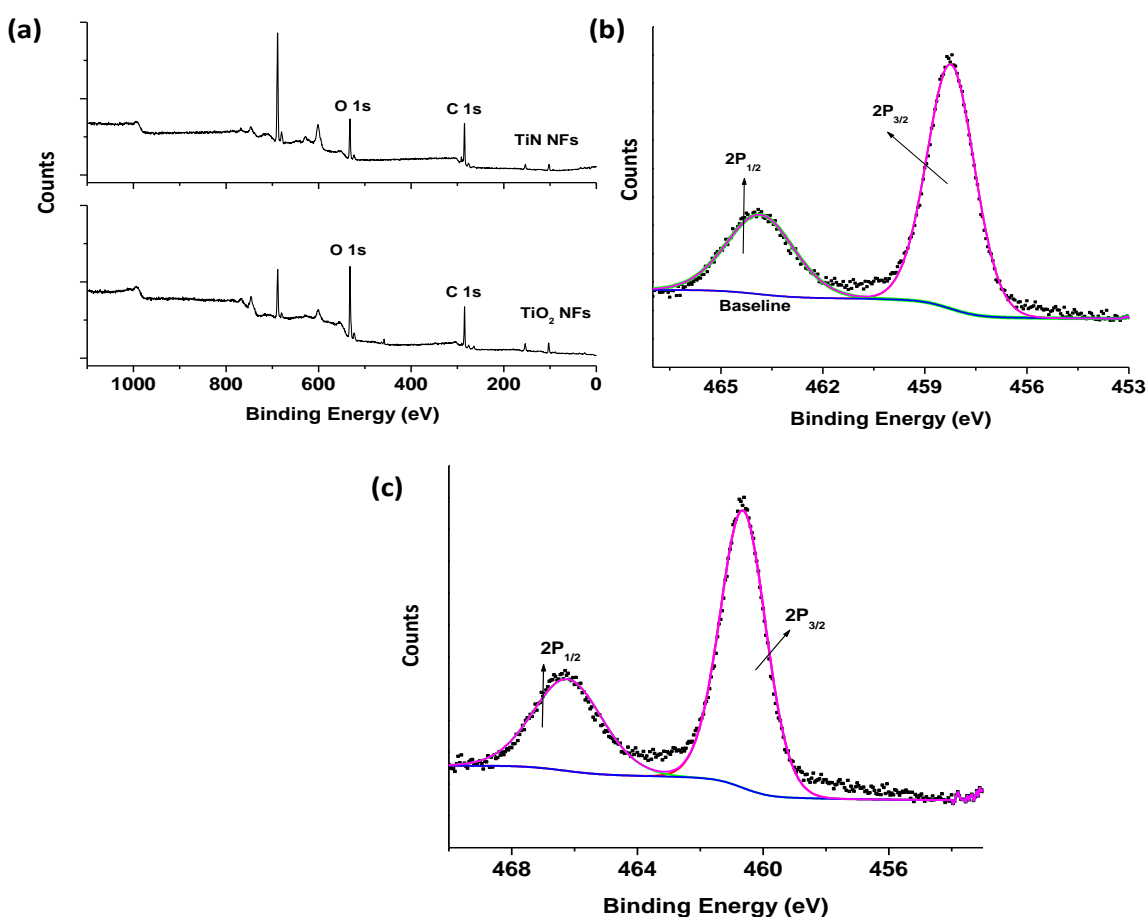


Figure S5. (a) Wide-scan spectra of TiO₂, and TiN NFs on glass substrate in a range of binding energy (0-1100 eV). The Ti 2P core-level XPS spectra for TiO₂ NFs (b) and TiN NFs (c).

Figure S5 provides the wide-scan XPS spectra for the synthesized TiO₂ and TiN NFs (Fig. S5a), and the 2P core-level XPS spectra for TiO₂ (Fig. S5b) and TiN NFs (Fig. S5c) which were deconvoluted into the

characteristic peaks using Shirley type baseline with Gaussian profile. The peaks for Ti $2p_{1/2}$ and Ti $2p_{3/2}$ spin-orbital splitting photoelectrons of TiO_2 were positioned at 463.8 and 458.3 eV, respectively (Fig. S5b). The peak for $2p_{1/2}$ at 463.8 eV was ascribed for Ti-N bonds in TiN NFs. After conversion of TiO_2 to TiN NFs, the peak due to Ti $2p_{1/2}$ was shifted to 3.9 eV towards higher binding energy after nitrogen incorporation (Fig. S5c).

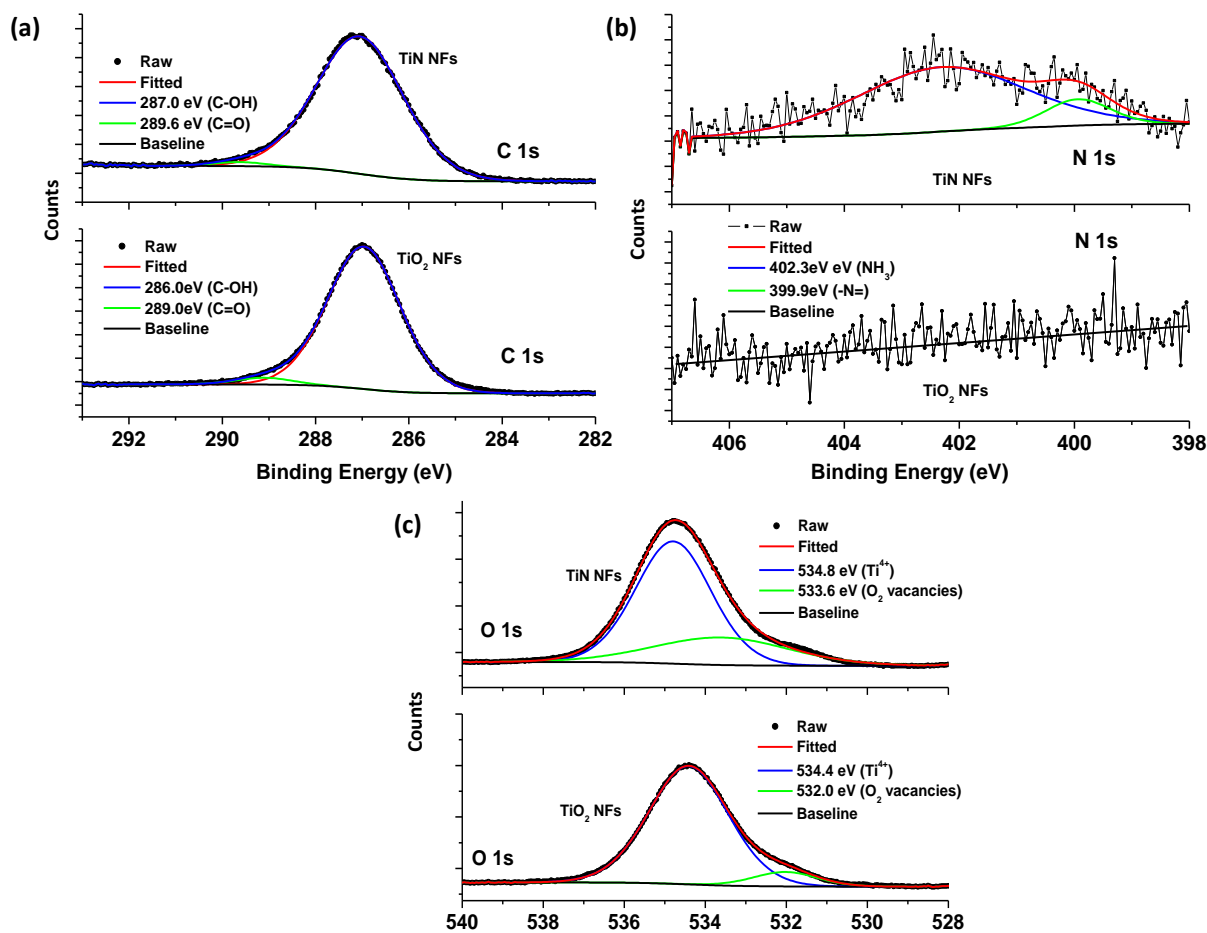


Figure S6. XPS core-level spectra of C 1s (a), N 1s (b) and O 1s (c) for TiO_2 and TiN NFs. The existence of C 1s peak at binding energy of 286.0 for TiO_2 is due to C-OH arising from the polymer during synthesis of TiO_2 NFs (Fig. S6a). This peak shifted to higher binding energy (287.0 eV) in case of TiN NFs due to nitrogen doping in TiO_2 and a small peak at 298 eV appeared after NH_3 gas treatment in TiO_2 . Further, nitrogen doping in TiO_2 NFs was confirmed by N1s spectra as shown in Fig. S6b. There was no trace amount of nitrogen found for TiO_2 NFs. TiN NFs had two peaks at 399.9 eV binding energy indicating that the core-level electron of N 1s and at 402.3 eV was due to absorption of NH_3 gas. In O 1s spectra of TiO_2 (Fig. S6c), the binding energy observed at 534.4 eV corresponded to oxygen bound to Ti^{4+} ions in TiO_2 , while binding

energy locating at 532.0 eV may be due to O₂ deficiencies of TiO₂. With nitrogen doping in TiO₂, however, the XPS peak for O₂ remained, which may be due to the surface of TiN on the glass substrate partially covered with hydroxide (OH) groups (Fig. S6c).

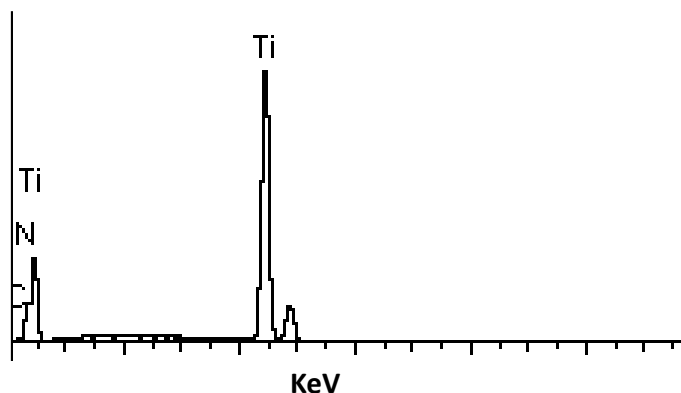


Figure S7. EDX spectra for elemental analysis of TiN NFs.

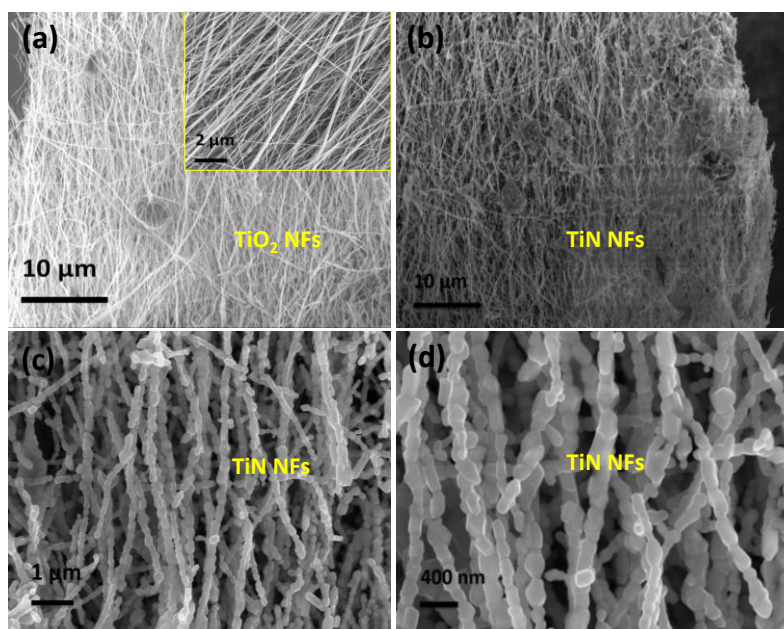


Figure S8. (a) FESEM image of electrospun TiO₂ NFs. Inset shows partially aligned TiO₂ NFs obtained by setting the flow rate of polymer concentration at 40 μL/min, the potential at 15 kV, and the distance between a tip and collector at 5 cm. (b-d) FESEM images of TiN NFs.

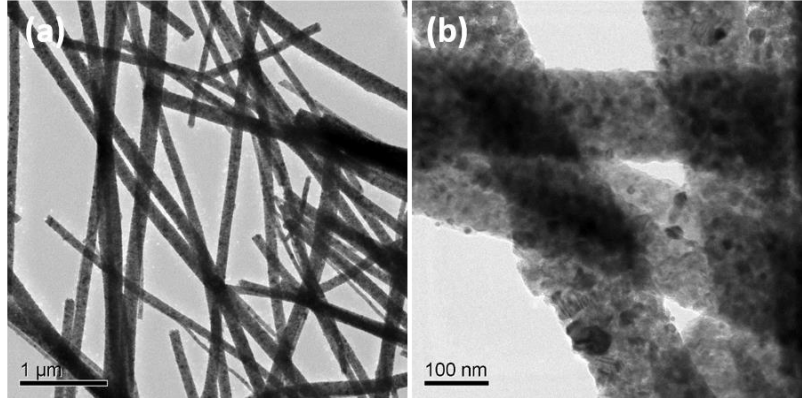


Figure S9. TEM images of TiO₂ NFs.

Table S1. Weight % and atomic % for synthesized TiN and TiO₂ NFs

	Elements	Weight %	Atomic%		Elements	Weight %	Atomic%
TiN NFs	C	1.87	5.95	TiO₂ NFs	C	4	6.5
	N	8.07	22.06		O	41	45.5
	Ti	90.0	72.00		Ti	55	48

Table S2. Electrochemical parameters of various electrodes.

Electrode materials	Current I (μA)	Diffusion coefficient D (cm ² /s)	Surface concentration Γ (mol/cm ²)	Heterogeneous electron transfer rate constant (k _s) (cm/s)
GF	-14	5.89×10 ⁻⁹	7.79×10 ⁻⁹	3.45×10 ⁻⁹
GF-TiN NFs	-75	1.69×10 ⁻⁷	41.7×10 ⁻⁹	4.01×10 ⁻⁹
NaR/GF-TiN NFs	-131	5.15×10 ⁻⁷	72.8×10 ⁻⁹	5.61×10 ⁻⁷

Randles–Sevcik equation is used to determine the diffusion coefficient D of ferro-ferricyanide and is given by^{S7}

$$I = (2.69 \times 10^5) n^{3/2} A D^{1/2} v^{1/2} c \quad \text{Eq. S1}$$

where I is peak current, D is diffusion coefficient (cm²/s), n is electrons transferred (n = 1), v is scan rate (mV/s), A is the geometrical area of electrode (0.096 cm²) and c is concentration (mol cm⁻²). Further, the surface concentrations of various electrodes were calculated using Brown–Anston Model and is given by

$$I = n^2 F^2 \Gamma A v / 4RT \quad \text{Eq. S2}$$

where F is Faraday constant (96,485.5 C mol⁻¹), A is surface area of the electrode (0.096 cm²), Γ is surface concentration (mol cm⁻²), v is scan rate (20 mV/s), R is gas constant (8.314 mol⁻¹ K⁻¹), and T is room temperature (298 K).

According to Laviron's theory, the heterogeneous electron transfer rate constant (k_s) can be calculated as⁵⁷

$$\log k_s = \alpha \log(1 - \alpha) + (1 - \alpha) \log \alpha - \log \left(\frac{RT}{nFv} \right) - \alpha(1 - \alpha) \frac{nF\Delta E_p}{RT} \quad \text{Eq. S3}$$

where α , R, T and F are the electron transfer coefficient (0.5), the ideal gas constant, the thermodynamic temperature, and Faraday constant, respectively. ΔE_p is the potential difference between the oxidation and reduction peak potentials.

References

- S1 P. LeClair, G. P. Berera and J. S. Moodera, *Thin Solid Films*, 2000, **376**, 9-15.
- S2 R. Krishnan, C. David, P. K. Ajikumar, R. Nithya, S. S. Tripura, S. Dash, B. K. Panigrahi, M. Kamruddin, A. K. Tyagi, V. Jayaram and B. Raj, *Journal of Materials*, 2013, **2013**, 1-5.
- S3 C. P. Constable, J. Yarwood and W. D. Munz, *Surf. Coat. Technol.*, 1999, **116**, 155-159.
- S4 P. W. Shum, K. Y. Li, Z. F. Zhou and Y. G. Shen, *Surf. Coat. Technol.*, 2004, **185**, 245-253.
- S5 Md. A. Ali, H. Jiang, N. K. Mahal, R. J. Weber, R. Kumar, M. J. Castellano and L. Dong, *Sens. Actuator B-Chem.*, **2016**, DOI: 10.1016/j.snb.2016.09.101.
- S6 R. Hood-Nowotny, N. Hinko-Najera Umana, E. Inselbacher, P. Oswald-Lachouani and W. Wanek, *Soil Sci. Soc. Am. J.*, 2010, **74**, 1018-1027.
- S7 R. Sharma, Md. A. Ali, N. R. Selvi, V. N. Singh, R. K. Sinha and V. V. Agrawal, *J. Phys. Chem. C*, **2014**, **118**, 6261-71.